Advanced Powder Technology 21 (2010) 663–675

Contents lists available at ScienceDirect

Advanced Powder Technology

journal homepage: www.elsevier.com/locate/apt

Original Research Paper

# X-ray micro tomography and image analysis as complementary methods for morphological characterization and coating thickness measurement of coated particles

Giacomo Perfetti [a,*], Elke Van de Casteele [b], Bernd Rieger [c], Willem J. Wildeboer [d], Gabrie M.H. Meesters [a,d]

[a] NanoStructured Materials Group, DelftChemTech DCT, Delft University of Technology, Julianalaan 136, 2628BL Delft, The Netherlands
[b] SkyScan NV, Kartuizersweg 3B, 2550 Kontich, Belgium
[c] Quantitative Imaging Group, Department of Imaging Science and Technology, Delft University of Technology, Lorentzweg 1, 2628CJ Delft, The Netherlands
[d] DSM Food Specialties, P.O. Box 1, 2600 MA Delft, The Netherlands

ARTICLE INFO

*Keywords:*
X-ray micro tomography
Image analysis
Film coating
Coating thickness
Coating morphology

ABSTRACT

This work demonstrates the potentiality of X-ray micro tomography as a powerful tool for morphological characterization of coated particles and, in particular, of their coating layer. X-ray micro tomography provides a high level of details at both micro and macro-scale. It was, in this work, used in the determination of density, porosity, surface/volume ratio, and thickness of the coating layer. Special emphasis was put on evaluation of the adhesion core/coating shell due to its strong influence on the acceptance and goodness of the final coated compound. Different definitions of coating thickness are evaluated. The variance of these properties is assessed within particles and between particles. A novel protocol was developed in order to segment the coating shell out from the core particles. The segmented out images were used to create 3D models of such coating shells. General aspects of theses models are discussed. The potential and limitations of X-ray micro tomography are finally highlighted based on the experimental work. Image analysis was used to determine the coating thickness applied on the core particles as complementary and reference method. As case study, two series of coated particles, prepared using top-spray fluidized bed coater, were obtained, each one employing three standard well-know coating agents.


## 1. Introduction

Aqueous film coating is a process commonly employed in the food and pharmaceutical industries. Agglomerates, granules, tablets, pellets and nonpareil seeds are often coated with polymers in order to control the dissolution of drug from the dosage form to give the product specific functionalities. Microencapsulation is a very popular method for the preparation of coated particles and, in general, for controlled release systems. Since small changes in processing parameters have the potential to greatly affect the properties of the final product, a rapid and non-destructive analytical method which detects these differences and gives an indication of the final product characteristics could be employed profitably as a quality control tool. Examples of these characteristics are: the thickness of the coating applied and the surface area of the coating shell [1,2], intra and inter-coating thickness uniformity and homogeneity [3], adhesion core-coating shell [4,5] and micro-level structure of the coating layer (e.g. porosity, micro-cracks, air bubbles). For many reasons it is of interest to assess the above mentioned parameters and to confirm non-ambiguously the quality of the both coating process and coating shell. In fact, evaluating the properties of coatings has the double purpose of assessing the adequacy of the process controls and ensuring the optimal performance of the final product.

Several techniques are currently available for coating analyses which provide the spatial resolution necessary for thin coating layer uniformity and structure measurements as well as prediction of coating thickness.

The most widely used techniques to visualize coated particles, coating structure and thickness, surface morphology are conventional light microscopy (LM) and scanning electron microscopy (SEM) [6–8]. Among several applications, Atomic Force Microscopy (AFM) studies surface roughness. Other methods are near-infrared (near-IR) spectroscopy [1,9–11] and laser profilometer [12] that are fast and highly accurate. Alternatively, a technique that potentially can be used for routine in-process testing of coatings is Laser Induced Breakdown Spectroscopy (LIBS), which has the potential to provide both rapid in-line analyses of multiple samples as well as the necessary spatial resolution [13]. X-ray photoelectron

* Corresponding author. Tel.: +31 15 278 43 92; fax: +31 15 278 49 45.
*E-mail address:* g.perfetti@tudelft.nl (G. Perfetti).

0921-8831/$ - see front matter © 2010 The Society of Powder Technology Japan. Published by Elsevier B.V. and The Society of Powder Technology Japan. All rights reserved.
doi:10.1016/j.apt.2010.08.002

spectroscopy (XPS) is a powerful technique widely used for the surface analysis of materials mainly, but it has also been used for coating thickness estimation [14]. Confocal scanning laser microscopy (CLSM) [15–21] minimizes scattered light from out-of-focus structures, and permits, through use of different fluorescence labels [22], not only analysis on the surface but also inside the material [23].

X-ray micro tomography is a relative new technique developed in the late 1970s, which enables the non-destructive, three-dimensional, visualization of the internal structure of objects [24,25]. It is based on the interaction of X-rays with matter. When X-rays pass through an object they will be attenuated in a way depending on the density and the atomic number of the object under investigation and of the used X-ray energies. By using projection images obtained from different angles a reconstruction can be made of a virtual slice through the object, non-destructively. By implementing mathematical algorithms, X-ray micro tomography creates cross-sectional images of the internal structure of the object. When these different consecutive slices are reconstructed a 3D visualization can be obtained with high resolution.

The objective of this study was to demonstrate the feasibility of X-ray micro tomography to successfully quantify film coating quality and to show the capability of this technique for measuring the thickness, its uniformity, the porosity, the density, the volume and the surface of a polymeric coating on not-spherical core particles. Particular attention was put on the valuation of the internal structures of coating layer as well as the interface core-coating shell. First a theoretical description of the technique is presented then its performance will be illustrated by both the quantification of coating quality and the calculation of coating thickness of coated particles produced via top-spray fluidised bed coating. The particles were coated by aqueous solutions of three different polymer materials and three coating levels. Two types of core particles were used. The present work aims also to demonstrate the simplicity and speed of this procedure as well as the value of the additional information that could be obtained by simple analysis.

## 2. Experimental section

### 2.1. Materials

Polymer-coated sodium benzoate and microcrystalline cellulose particles were chosen as a model system for this work. The sodium benzoate, Purox-S®, was supplied by DSM, Geleen, The Netherlands while the microcrystalline cellulose Cellets 1000 was provided by Syntapharm, Mülheim an der Ruhr, Germany. Their particle sizes, after sieving, were approximately 1150 and 1200 μm for Purox-S and Cellets, 1000, respectively. PolyVinyl Alcohol, PVA, (Mowiol® 4-98, Sigma–Aldrich, UK) with an $M_w$ of 27,000, a viscosity of 4–4.5 Pa s (3% solution in water at 25 °C) [26], and two grades of HydroxyPropyl MethylCelluloses, HPMC, (Pharmacoat® 603 and Pharmacoat® 615, Syntapharm, Mülheim an der Ruhr, Germany) with a $M_w$ of 13,000 and 65,000 and a viscosity of 4.5–5 and 29–31 Pa s [26], respectively were used, as received, as coating agents. The three film forming agents are referred to as PVA 4-98, HPMC 603 and HPMC 615 further in this article.

### 2.2. Preparation of solutions and particle coating

The aqueous solutions of PVA 4-98, HPMC 603 and HPMC 615 at 3% weight content as well as the top-spray fluid bed coating processes were performed as described previously [27]. Neither additives nor plasticizers were added to the solutions. All the polymers were used without any pre-treatment and the coating solutions were obtained according to supplier's specifications.

### 2.3. Scanning electron microscopy, SEM

Scanning electron microscopy is an effective method for qualitative analysis of the surface structure and morphological homogeneity of the coating shell. All images were produced with secondary electrons using a Philips XL 20 Scanning Electron Microscope (electron source from conventional tungsten's filament) operated at an acceleration voltage of 15 kV. Samples were prepared by attaching approximately 15 particles to a metallic support with araldite adhesive and a thin layer of gold was applied using an Edwards Sputter Coater (pulse mode, 6 min plasma coating) to improve the conductivity and reduce charging.

### 2.4. X-ray micro tomography

For the micro tomography measurements the SkyScan 1172 was used. This is a high resolution desktop X-ray micro-CT system with a closed X-ray micro-focus source. The maximum peak voltage of this tube is 100 kV with a maximum power of 10 W. It has a Tungsten reflection target and a focal spot of 5 μm. The detection system consists of a gadox ($Gd_2O_2S$) scintillator with a 2:1 fibre optic coupling to a $4000 \times 2096$ large format 12-bit cooled CCD camera.

The particles under investigation were put in a small Plexiglas container with an inner diameter of 3.5 mm. This sample holder was placed between the X-ray source and detector where the distance of the sample holder to the source determines the magnification of the system as a consequence of the cone beam of the source. This magnification will be set so that the container stays within the field of view of the detector for the full rotation cycle. In order to get high resolute images by X-ray micro tomography the diameter of the sample is of utmost importance and represents the key factor of the imaging process. By using the Plexiglas container it was possible to scan several particles at once and still obtain a good pixel resolution. With the camera binning of 2 by 2 pixels taken together giving 2000 pixels on a row instead of 4000, an isotropic pixel resolution of 2 μm was obtained. In Fig. 1a and b a projection image of the coated Purox-S and Cellets 1000, respectively, in the Plexiglas container can be seen.

Since the particles have a low density, an optimal contrast can be obtained using the lower X-ray energy part of the X-ray spectrum. This can be done by setting the peak voltage of the source at 40 kV with a current of 250 μA. Projection images were taken every 0.4° rotation step over 180°. To improve the signal to noise of the projection images a frame averaging of 3 was taken.

After the acquisition of the projection images the reconstruction was done using a modified Feldkamp cone beam algorithm [28]. Finally the 2D cross-sectional images of the sample were obtained in consecutive slices throughout the object. This 3D dataset can then be viewed in any direction as shown in Fig. 1c and d for coated Purox-S and Cellets 1000, respectively.

The entire acquisition took approximately 35–40 min with an exposure time of 590 ms per projection. After acquisition of the projection images, the reconstruction was performed and a series of 489 2D cross-sectional images of the specimen were obtained in consecutive slices throughout the object (Fig. 2a). Once the Region of Interest, ROI, has been chosen (Fig. 2b), the coating shells were segmented out. Only pixels belonging to the coating shell were taken into account for further calculations. After the segmentation process the coating shells were threshold and black–white (binary) images were obtained (Fig. 2c). After coating shell binarization, we generated 3D visualisations of the polymer coating shells (Fig. 2d). Investigation of the 3D structure leads to further information about the quality of the structure in terms of eventual orientation, porosity, density and core-coating layer adhesion, and thus, more in general, about the quality of the coating process.

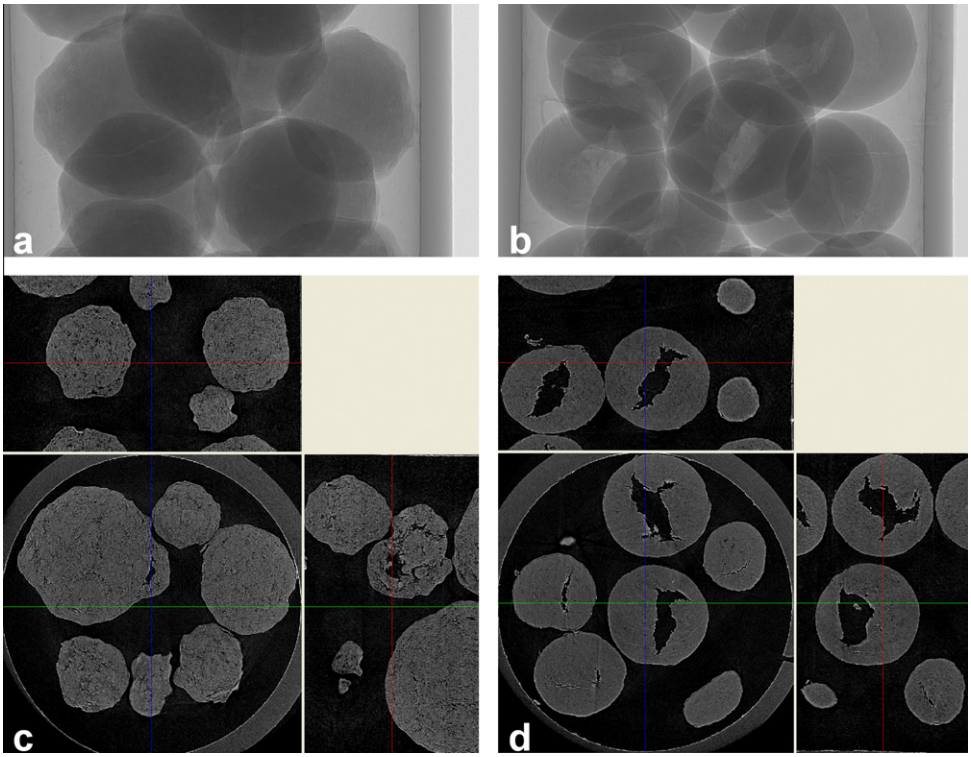


**Fig. 1.** Projection image of the sample in the scanner (a and b), and longitudinal, sagittal and transversal sections of X-ray tomography 2D cross-sectional images (c and d) for Purox-S (a and c) and Cellets 1000 (b and d) coated particles.

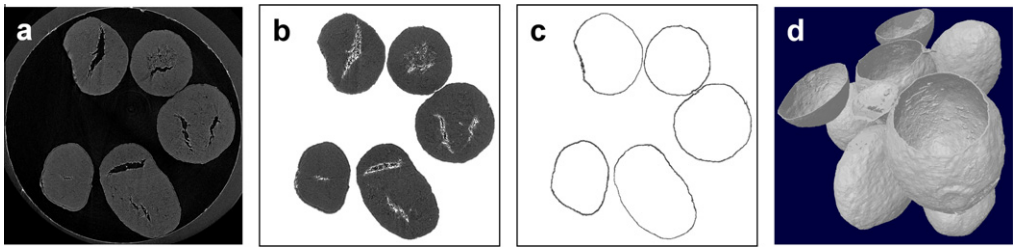


**Fig. 2.** X-ray tomography experimental protocol: projection image (a); projection image once the Region of Interest has been identified and selected (b); coating shell after thresholding and segmentation processes (c); 3D reconstructed model of the batch analysed (d).

### *2.5. Structural and morphological parameters of coating shell*

The studies presented in this article also focus on gaining a systematic understanding of the influence of the coating process on microstructure characteristic of the coating shell. The influence of the core particles, the coating material and the coating level finally applied on the morphology and microstructure architecture of the coating shell were studied. To do this, a fully quantitative microstructure characterization of the 3D generated model was carried out. The knowledge of the structure and architecture of the coating shell is of primary importance when evaluating the quality of the final product as well as the control of the process used to apply the coating. Moreover it gives relevant information when addressing specific requirements. The images of the coating shell obtained from X-ray tomography were used to obtain a number of important parameters [29] such as:

(1) the ratio solid surface-volume $\beta$ ($\mu m^{-1}$);
(2) the surface density $\rho$ ($\mu m^{-1}$);
(3) the number of pores $\Phi_{num}$, in the coating shell and the corresponding volume $\Phi_{vol}$ ($\mu m^3$), occupied by the pores;
(4) the percentage porosity $\Phi$ (%).

In this study the ratio solid surface to volume $\beta$, is measured in 3D within the Volume of Interest (VOI) and represents a useful basic parameter for characterizing the thickness and the complexity of structures. In this regard it is considered as a measure for the roundness and roughness of the coating shell. For a specified coating level, the rougher the external surface of the coating shell is, the higher the ratio, on the contrary, the smoother the surface, the lower the ratio. Similarly, considering a certain amount of coating applied, the higher the roundness of the coated particles, the lower the external surface and thus the lower the ratio which evidently corresponds to spherical and smooth coating surfaces. Moreover, the ratio $\beta$ can be also considered as an indirect measure of the coating quality and uniformity. In fact, the smaller the solid volume of the coating shell is, i.e. the higher the number of inaccuracies like air bubbles, and pores, the higher this ratio, the worst the coating quality is.

The surface density $\rho$, is calculated as the ratio of surface area of all the solid objects within the Volume of Interest (VOI) measured in 3D using Marching cubes method [30] to the total volume of Volume of Interest (VOI).

A discreet 3D pore is a connected assemblage of space being all black voxels that are fully surrounded on all sides in 3D by solid,

white voxels. According to this definition the number of pores $\Phi_{num}$, is calculated as the total number of discreet pores within the VOI. Note that according to this definition of a pore, a space located within a solid object or between solid objects, but which has any connection to the space outside the object or objects, is not identified or measured as a pore.

The percent porosity $\Phi$, is the volume of pores as percent of the total of solid plus pore volume, within the Volume of Interest measured in 3D.

The assessment of these parameters allow, in addition to obtaining single values, to also quantify coating uniformity, homogeneity of the structure as well as to evaluate whether or not coating imperfections occurred. Additionally, in order to compare the different experiments at both coating material and coating level, the values of the parameters just mentioned above, obtained from the analysis of 3D reconstructed images of single particles were averaged over all batches.

### 2.6. Coating thickness

Three different approaches were used to measure the thickness of the coating shell. In the first one the Theoretical Experimental Thickness was assessed by using an experimental equation and the results were used as reference values. In the second and third approach the 2D reconstruction images and 3D reconstructed images obtained from X-ray tomography were analysed by means of image analysis processing tools. For the second approach, image analysis software was employed (CTAn, SkyScan) and three different definitions of thickness were evaluated, namely cross-sectional thickness from 2D Analysis, structure thickness from 2D analysis and structure thickness from 3D analysis. For the third approach, where Matlab (The Mathworks, USA) and DIPimage (Delft University of Technology, www.diplib.org) were used, three different definition of coating thickness were evaluated also.

It will be shown below that these methods allow, in addition to obtaining values for the mean coating thickness, to also quantify coating thickness uniformity, and thus, 2D and 3D coating thickness distribution all around the particles. Moreover, possible variances of coating thickness both within the particle and within the batch and eventual zero-coating spots are also presented.

#### 2.6.1. Theoretical experimental thickness

The theoretical reference coating thickness was calculated using the equation proposed by Dewettinck et al. [31] which is as follows:

$$d_s = r_m - r_c = \left[\left(\frac{w_s}{w_c}+1\right)^{1/3} - 1\right] r_c \quad (1)$$

where $d_s$ is the theoretical coating thickness (m), $r_c$ is the radius of core particle (m), $r_m$ the radius of the coated particles (m), $w_s$ the weight of the coating material (g), $w_c$ the weight of the core material (g). The equation is based on the assumptions that all core particles are considered perfectly spherical, they all have the same identical particle radius, $r_c$, no coating losses occur during the process and that a coated particle can be approximated as two concentric spheres one on top of the other.

#### 2.6.2. Image analysis approach

*2.6.2.1. Software package: CT analyser.*

*2.6.2.1.1. 2D Cross-sectional thickness.* The cross-sectional thickness $T_h$, is calculated after thresholding of the reconstructed images on the basis of the "plate model" in 2D [32] according to the following equation:

$$T_h = \frac{2}{S_s/V} \quad (2)$$

where $S_s$ is the surface area of the solid object within the volume of interest, and $V$ the volume of the object within the volume of interest both measured in the 2D cross-sectional image using the Pratt algorithm [33].

The cross-sectional thickness is a calculation of thickness in which the vertical surfaces, between pixels of adjacent cross-sections, are excluded; only the perimeters of cross-sections are used to calculate surface. This definition of surface excludes error caused by large artificially cut surfaces that sometimes occur at the top and bottom of Volumes of Interests. In order to compare different coating material as well as different coating levels, the individually mean values from all 2D reconstructions images obtained for each particle in the sample were averaged and reported together with the maximum and minimum values (inter-particles uniformity). To estimate the intra-particle variation (intra-particle uniformity) of the coating thickness, the average standard deviation within all the reconstructed images for each individual particle was calculated.

*2.6.2.1.2. 2D Structure thickness.* The 2D structure thickness calculation is based on Eq. (2). In contrast to cross-sectional thickness, the structure thickness 2D includes surface, between pixels of adjacent crossections, measured both vertically and horizontally which yields to smaller thickness values. It is important to highlight that this value, because of model assumption, only provides us with a hypothetical "true" thickness. The closer to the reality the model is, the more realistic this measurement.

*2.6.2.1.3. 3D Structure thickness.* The true 3D, model independent, thickness was measured using the threshold reconstruction images of each individual coating shell. In this case the 3D structure thickness is based on the definition of Hildebrand and Ruegsegger [34]. Let consider an arbitrary local point within the coating layer. The 3D structure thickness is defined as the diameter of the largest sphere which contains the considered point and which is completely inside the coating layer ("sphere fitting"). Being the 3D structure thickness defined for all the points of the 3D structure, it is here referred as volume-based local thickness.

Distance-transform methods described by Remy and Thiel [35] are the basis for the implementation by CT analyser of local thickness measurement. The method starts with a "skeletonisation" identifying the medial axes of all structures. These curve skeletons are a set of one-dimensional curves that are locally symmetric with respect to the shape boundary. The obtained skeleton is a compact representation of the coating shape that maintains its topology. Then the "sphere-fitting" local thickness measurement is made for all the voxels lying along this axis. The coating thicknesses values of all particles within the batch were then averaged in order to have one reference 3D thickness value characteristic for the batch.

*2.6.2.2. Matlab and DIPimage.* The reconstructed images obtained by X-ray micro tomography were also independently analysed, over the segmented coating shells, using Matlab-DIPimage image analysis software to check on the accuracy of coating thickness measurements obtained from the CTAn. After segmentation the volume of coating layers are threshold to generate a binary mask image in that sense that all non-zero pixels are assigned as foreground. From this segmentation the coating thickness will automatically be computed for each particle in all images. By using Matlab (The Mathworks, USA) and DIPimage (Delft University of Technology) as tools for image processing, particles are fully automatically identified in the following manner.

We assume that particle coating segmentations are non-touching in the lowest z-slices. From that overlapping objects in the subsequent z-slice are assigned to the same particle by overlap. If

there is no overlapping object in the prior slice, a new particle is added. We only consider segmented particles which contain at least 100 voxels in each slice. In the xy-slices we use an 8-connected neighbourhood for the labelling of the objects. Touching particle coatings are separated automatically (most of the times successfully) by filling the particles via binary morphological operations [36] then computing a distance transform from the outside. If now two disk-like particles touch, the distance transform will have a very low value at the touching location. A watershed operation [37] will now isolate the two peak values in the middle of each particle and draw a border through the touching region. This border is used to separate the two touching particles.

Once the particles have been assigned unique labels in the volume we can measure the thickness of the coating layers. Three definitions, namely *Avg2D*, *Surf2D* and *Surf3D*, have been implemented and used to measure coating thickness:

(1) *Avg2D:* a 2D approach where the coating thickness is measured in each 2D slice of the reconstructed volume as one average value.
(2) *Surf2D:* a 2D approach where the coating thickness is measured in each 2D slice of the reconstructed volume as a function of the position on the coating.
(3) *Surf3D:* a 3D approach where the coating thickness is measured in the reconstructed volume as function of the coating surface together with its intra-particle standard deviation. The 3D coating thicknesses values of all particles within the batch were then averaged in order to have one reference 3D thickness value characteristic for the batch. Maximum and minimum values as well as the intra-batch standard deviations, as measure of the thickness uniformity within all the particles in the batch, were obtained.

For each particle coating the binary skeleton is computed, i.e. a one pixel thick, connected line in the middle of the coating. For the definition Avg2D the average thickness in each xy-slice is computed as the number of foreground pixels divided by the length of the binary skeleton as in good approximation the area is length per thickness. In approach Surf2D, the thickness is determined locally as the extend of the coating layer perpendicular to the surface at a given point. This is achieved by computing the gradient vector on each xy-position of the binary skeleton image. The thickness is then determined in the direction of this gradient. We walk along the gradient and stop if the pixel value is not larger than 0.5. For the definition Surf3D the same procedure as for Surf2D is used but now on xyz-positions of the binary skeleton image and the gradient is computed in the volumetric image. As the volumes are rather large ($\sim 800 \times 800 \times 500$ pixels) computation in 3D requires at least 8 GB of main memory to hold the different images and perform computations. The algorithms have been tested on artificially generated binary spheres-shells of different thickness in the range 1–6 pixels and outer radii of 20, 30, 40, 50 and 60 pixels.

## 3. Results

Two types of HydroxyPropyl MethylCellulose, HPMC 603 and HPMC 615, and Polyvinyl Alcohol, PVA 4-98, were used as coating agents for top-spray fluidised bed coating of both Purox-S, and Cellets 1000 as core materials. Coated particles were obtained at three different coating levels, namely 1%, 5% and 9% w/w. As a first step of this part of the work, the quality and reliability of the X-ray tomography technique for looking at the structure characteristics of polymer-coated pellets was proven. The overall quality of the images was discussed and both strengths and weaknesses are highlighted. Then coating layer thickness as well as structural and morphological parameters is measured. Scanning electron microscope (SEM) was employed as reference and comparison.

### 3.1. X-ray tomography

#### 3.1.1. Reconstructed 2D images

As first aim of this part of work, the quality and reliability of X-ray tomography technique for looking at the structure characteristics of polymer-coated pellets was proven. The overall quality of the images is discussed and both strengths and weaknesses are highlighted.

A population of ±25 particles per batch was taken into account. Considering the standard size of the coated particles, 1150 ± 15 and 1200 ± 15 μm for Purox-S and Cellets 1000, respectively, and the scan size, 1 μm, the scanning step resulted in a very large datasets of 575 ± 8 and 600 ± 8 acquired reconstruction images for Purox-S and Cellets 1000 respectively.

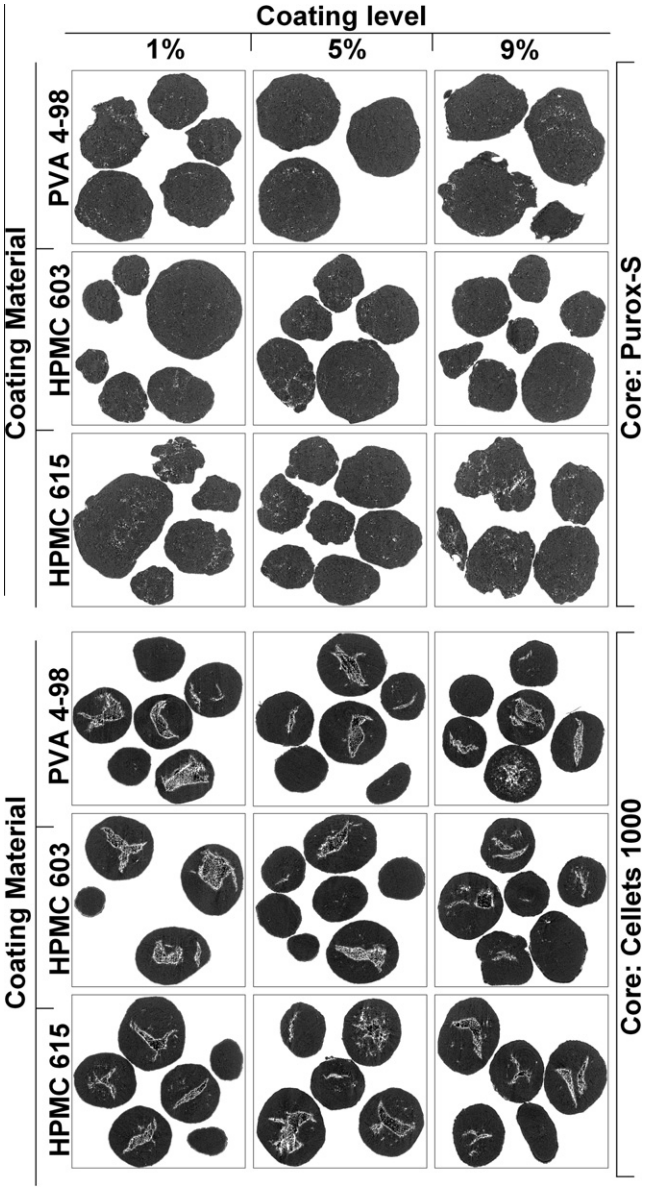


**Fig. 3.** Reconstructed images of Purox-S (top part) and Cellets 1000 (bottom part) coated with PVA 4-98 (1st row), HPMC 603 (2nd row) and HPMC 615 (3rd row) for 1 (left column), 5 (centre column), 9% (right column) w/w coating after reconstruction and definition of Region of Interest, ROI.

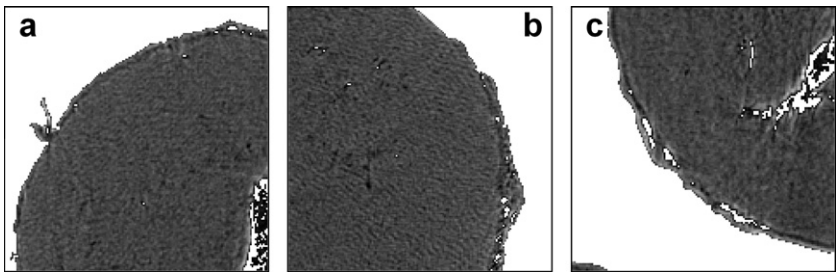


**Fig. 4.** Zoomed in X-ray tomography projection images of Purox-S coated with 9% w/w PVA 4-98 (a), HPMC 603 (b), HPMC 615 (c).

Fig. 3 shows reconstructed images of Purox-S and Cellets 1000 coated with PVA 4-98, HPMC 603 and HPMC 615 for 1%, 5%, 9% w/w coating obtained after acquisition of the projection images (consecutive slices throughout the object) and reconstruction process (within the ROI). The overall quality, in terms of resolution, focus and sharpness of the images resulted to be good. Thanks to the different density and atomic number of the coating agents compared to the core particles (black-like part) the coating shell (grey-like part) can be indentified. However, in general, a much better contrast, in colour and density, between core and coating could be detected for Cellets 1000 coated particle than Purox-S.

Due to the white background of the surroundings, in contrast with the grey one of the core particle, the difference in intensities is greater at the outer border of the coating shell than at the inner one, making the visualization of the outer border of the coating shell much easier than the inner border. At the inner border the coating was only slightly different in texture from the core, but with a clear difference in colour. The absolute colour of the coating shell only varies within pellets and between pellets. However quite relevant differences could be noticed between coating agents and, within the same coating agent, when spraying different amount of coating solution.

To almost perfectly spherical shape of Cellets 1000 corresponds a more irregular shape of Purox-S. This conformation influences, of course, the final shape and structure of the coating layer. In fact, the architecture of the coating shell is defined by the form of the core particle especially in cases of thin coating shells. The more coating is applied the more spherical and regular the external shape of the coated particle becomes. Big empty regions are visible within the core of the Cellets 1000 (Fig. 3, bottom part), which are, on the contrary, not present in the structure of the Purox-S (Fig. 3, top part). Such "holes" are mainly noted in the central region of the Cellets 1000 and their shape changes particle by particle. Nevertheless the structure looks homogeneous in density not showing cracks and imperfections. Empty holes apart, Cellets 1000 looks much denser and compact than Purox-S which has small but numerous cavities well distributed all over its structure. Some imperfections and agglomerated features are also visible.

X-ray micro tomography allows one to investigate the actual adhesion-connectivity between the core particle and the coating material once the latter has been sprayed. The magnified images in Fig. 4 show the interface between core and coating shell for both Purox-S (Fig. 4a and b) and Cellets 1000 (Fig. 4c) coated particles. In both Purox-S and Cellets 1000 coated particles, some macro-porosity is visible in the coating shell structures as well as some fractures and micro-fractures, probably due to handling and impact during coating process. However, the distribution of the porosity is not homogeneous, which is related to the sample preparation. The adhesion is extremely poor in certain regions. In fact, independent of the coating material, in certain cases the coating shell is completely disconnected from the core material (Fig. 4b and c). Moreover we can also distinguish areas where no coating has been applied (Fig. 4a and b). Several reasons might determine such poor adhesion as the spreading mechanism of the coating solution during the spray process dependant of fluid bed temperature, the viscosity and the concentration of the coating solution, the dimension of the droplets and many variables more. The possibility of looking deeply at the interface core-coating layer is of considerable interest in determining the mechanisms of coating solution's spreading, to

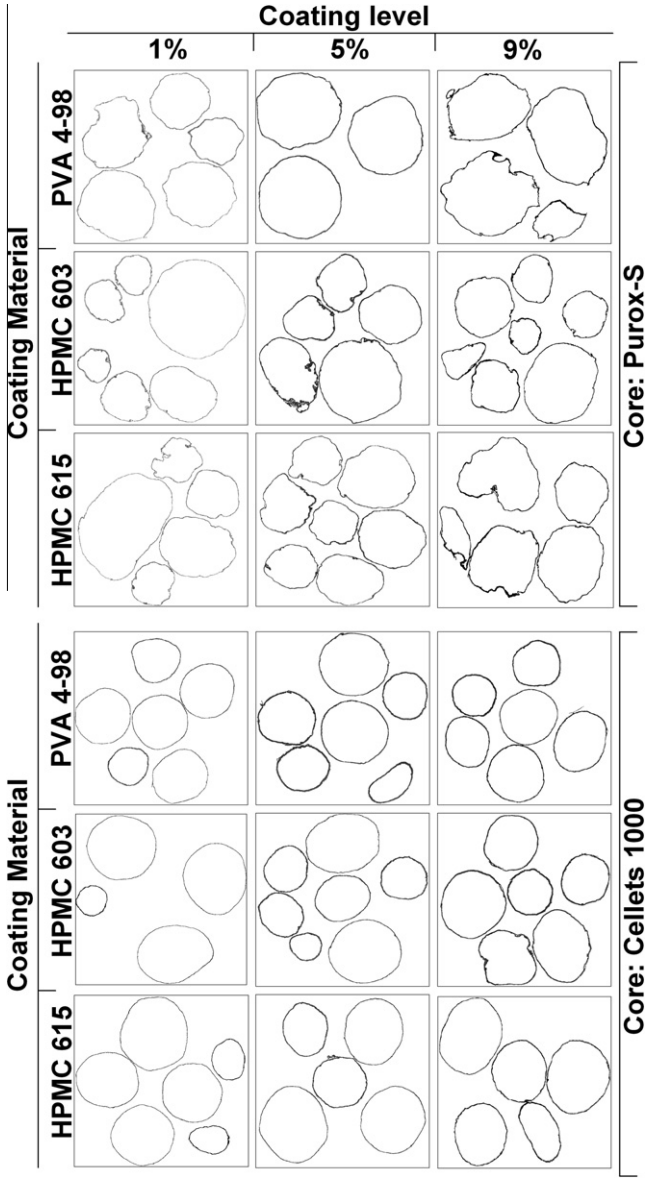


**Fig. 5.** X-ray tomography images of segmented out coating shells of all batches analysed. Influence of core material (left: Cellets 1000, right: Purox-S) and coating fraction applied (1–5% to 9% w/w from left to right) per each set of images.

localize weak points for possible crack generation as well as powerful tool for assessment of the quality of the final product.

*3.1.2. Segmented-out 2D coating layers*

The coating shells were then segmented out of their core particles. After applying the general auto-threshold process the coating shells (white, indicating the background, and black, identifying the coating shell) are now very visible and measurable. Fig. 5 depicts the coating shells of the obtained coated particles once they have been segmented-out.

*3.1.3. 3D model of coating shells*

After coating shell binarization, CT analyser was then used to process the 2D segmented-out reconstruction images to get the 3D models of all the batches analysed in this work which is shown in Fig. 6. It is, in fact, of a high interest to effectively visualize the 3D structure and the shape of the coating shells. A horizontal plane cut in the 3D reconstructed models was carried out in order to look inside the coating shells, at the interface between coating layer and core particle. Investigation of the 3D structure leads to further information about the quality of the structure in terms of eventual orientation, porosity, density and core-coating layer adhesion, and thus, more in general, about the quality of the coating process. This enables us to compare, qualitatively, the inner and outer structure of the coating shells and, therefore, to see how the coating has grown throughout the spraying process. These 3D reconstructions can be easily rotated, re-coloured, sectioned and processed to allow precise coating shell qualitative characterizations. Looking at the images depicted in Fig. 6 it becomes immediately clear that,

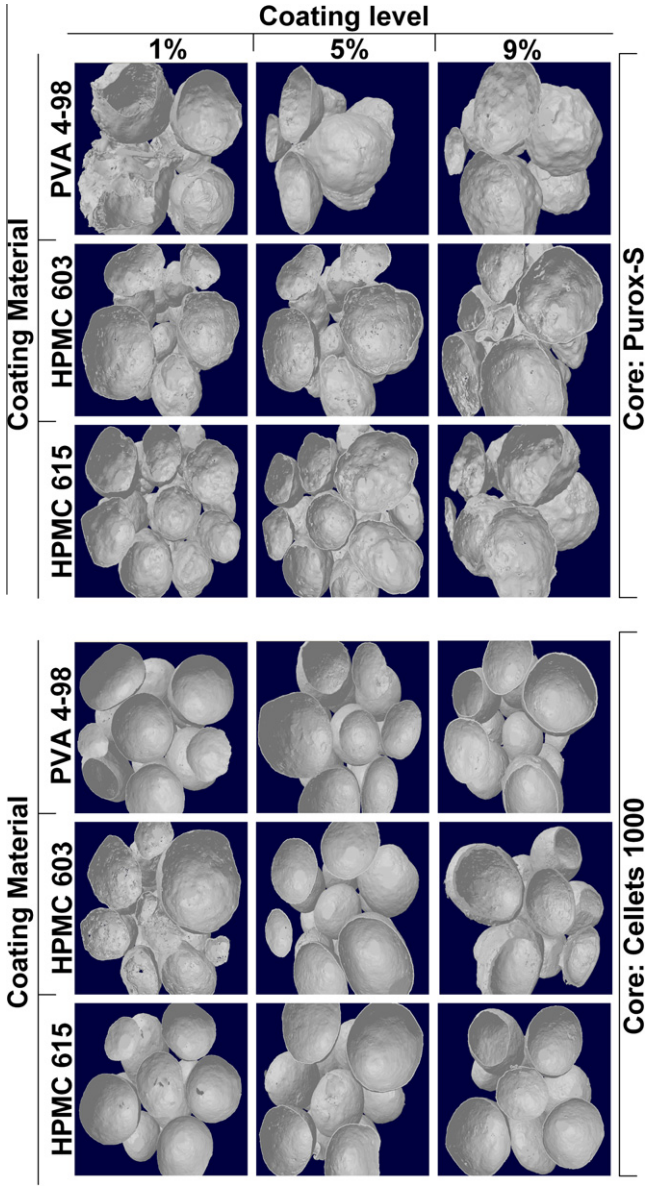


**Fig. 6.** 3D image reconstructions of coating shells for all experiments performed.

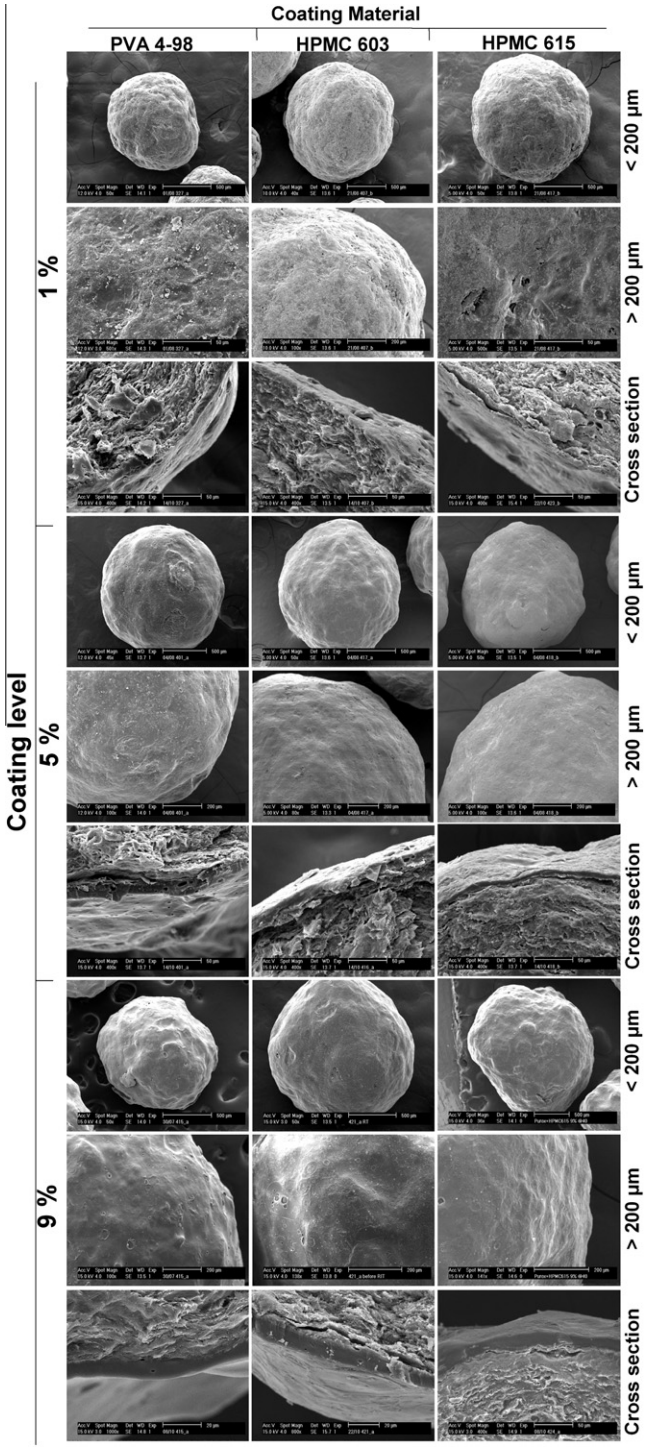


**Fig. 7.** Macroscale (>200 µm), microscale (<200 µm) and cross section SEM micrographs of Purox-S coated with PVA 4-98, HPMC 603 and HPMC 615 from the left to the right, 1–5% to 9% w/w coating level from the top to the bottom.

because of its initial quite perfect spherical shape, the coating shells applied onto Cellets 1000 are much more regular and smooth confirming the considerations drawn so far. On the contrary, the coating shells applied onto Purox-S present quite irregular shape, keeping, basically, the initial conformation of the uncoated Purox-S. Nevertheless the sphericity of the Purox-S coated particles is higher than that from the uncoated one. During the coating process, at the beginning of the spraying, the droplets tend to flatten the irregular surface of the Purox-S, by filling valleys, and, thus, leading to smoother and more spherical external surface. The zero-coating spots and irregularities, easily visible and quantifiable as the colour contrast between coating shell and background is pretty high, present in coated Purox-S are, in number, much more when compared to those in Cellets 1000.

Figs. 7 and 8 gather scanning electron microscope images of Purox-S and Cellets 1000, respectively, coated with 1–5% to 9% w/w PVA 4-98, HPMC 603 and HPMC 615 as reference. Per each coating material a macro-level (>200 μm), a micro-level (<200 μm) and a cross section picture are presented.

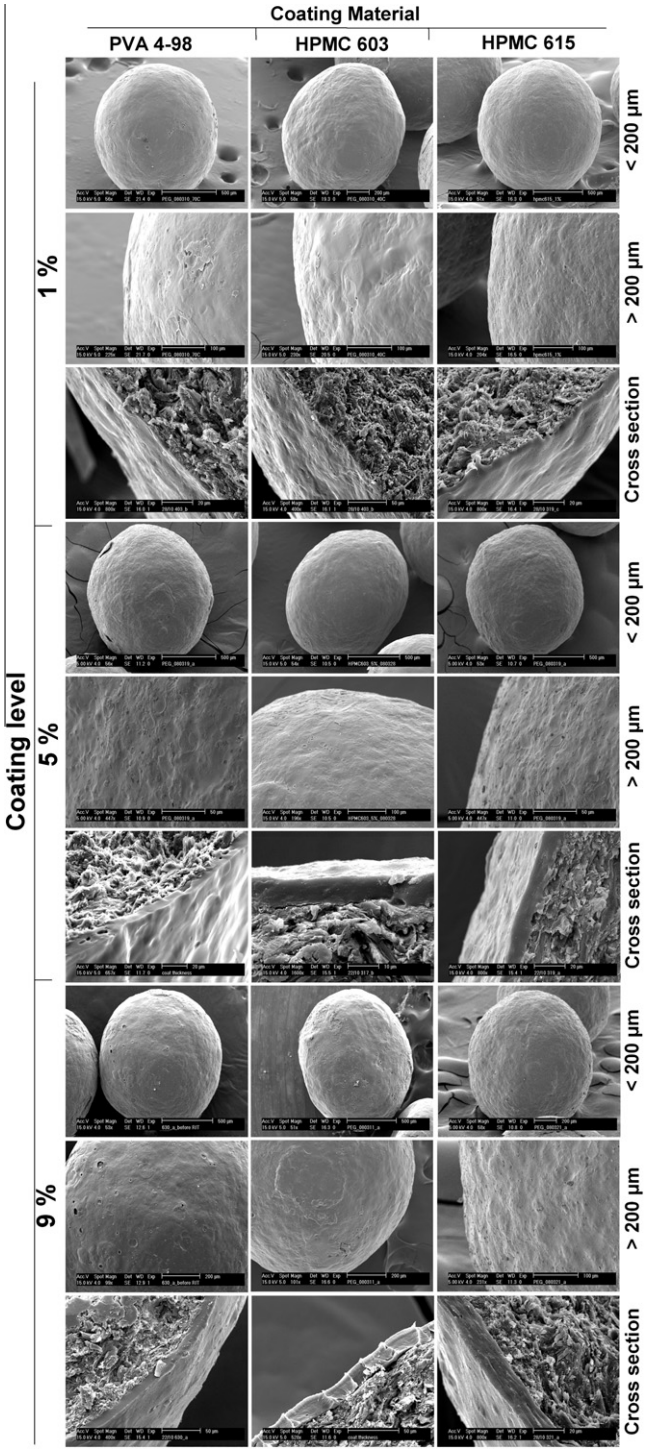


**Fig. 8.** Macroscale (>200 μm), microscale (<200 μm) and cross section SEM micrographs of Cellets 1000 coated with PVA 4-98, HPMC 603 and HPMC 615 from the left to the right, 1–5% to 9% w/w coating level from the top to the bottom.

### 3.2. Coating thickness

In this section the coating thickness is measured as function of the coating material, the coating level and type of core pellet.

#### 3.2.1. CT analyser

From Table 1, it can be seen that, according to the expectations, the theoretical coating thickness is increasing with increasing coating solution sprayed during coating process. Furthermore, it can be noticed that such increasing in coating thickness is not directly proportional to the coating fraction sprayed. The 3D structural thickness has been found to be approximately 2.5–2.7, 6.2–6.5 and 11.8–12.6 μm for 1%, 5%, 9% w/w coating level for Purox-S coated particles and 1.8–2.4, 6.01–6.8 and 12.5–12.9 μm for 1%, 5%, 9% w/w coating level respectively in case of Cellets 1000. Similar values have been found for the 2D Structural Thicknesses. No reliable trend could be established when comparing it to the 3D structural thickness though.

Overall, the 3D structural thickness and 2D structural thickness were in good agreement with the theoretical thickness especially for coating levels of 5% and 9% w/w. The differences of 1–2.5 μm have to be only partially adducted to measurements errors by the X-ray tomography. Mainly, this can be explained by an increasing of agglomeration and disturbed dynamics within the fluid bed reactor which might have lead to heavy losses in coating solutions while spraying. Because of this, consistent part of the coating solution is wasted and/or lost and, thus, the coating is thinner than the expected one from Eq. (1). Additionally, it is important to remind the readers that, when comparing the reference theoretical

**Table 1**
Coating thickness calculations for Purox-S and Cellets 1000 coated particles with PVA 4-98, HPMC 603 and HPMC 615 for 1%, 5% and 9% w/w coating level.

| Coating material | Coating level (% w/w) | Experimental equation | Image analysis: CT analyser | |
|---|---|---|---|---|
| | | Theoretical thickness (um) | 3D Structural thickness (um) | 2D Structural thickness (um) |
| *PUROX-S* | | | | |
| PVA 4-98 | 1 | 1.284 | 2.783 | 2.957 |
| | 5 | 6.614 | 6.499 | 6.775 |
| | 9 | 15.035 | 12.518 | 11.868 |
| HPMC 603 | 1 | 1.229 | 2.528 | 2.01 |
| | 5 | 6.334 | 6.282 | 6.156 |
| | 9 | 14.404 | 12.528 | 12.602 |
| HPMC 615 | 1 | 1.229 | 2.555 | 2.21 |
| | 5 | 6.334 | 6.46 | 6.816 |
| | 9 | 14.404 | 12.632 | 12.433 |
| *CELLETS 1000* | | | | |
| PVA 4-98 | 1 | 1.57 | 2.405 | 2.161 |
| | 5 | 8.094 | 6.198 | 7.447 |
| | 9 | 15.035 | 12.533 | 12.997 |
| HPMC 603 | 1 | 1.503 | 2.385 | 2.187 |
| | 5 | 7.75 | 6.01 | 6.856 |
| | 9 | 14.404 | 12.574 | 12.56 |
| HPMC 615 | 1 | 1.503 | 1.802 | 2.176 |
| | 5 | 7.75 | 6.843 | 7.176 |
| | 9 | 14.404 | 12.952 | 12.801 |

values for coating thickness to the X-ray tomography data, Eq. (1) is based on the assumption that all core particles are considered perfectly spherical, they all have the same identical particle radius, no coating losses occur during process and that a coated particle can be approximated as two concentric spheres one on top of the other. Moreover, as underlined by Depypere et al. [21] Eq. (1) assumes the exact knowledge of the coating material particle density. On the contrary, the 3D structural thickness and 2D structural thickness for 1% w/w coating level were all 0.5–1.3 μm higher than the theoretical thickness. These overestimations are due to the resolution limitation of the technique. 1% w/w coating level, in fact, gives coating thicknesses for which, using the selected X-ray settings for resolution and pixel size, a proper threshold and hence a proper thickness calculation was not possible.

In Table 2 the 3D structural thickness and 2D structural thickness (Section 2.6.2), obtained using the image analysis from CTAn, for Purox-S and Cellets 1000 coated particles are shown. Both the 3D structural thickness and 2D structural thickness were obtained as function of coating material, core particle and coating level (% w/w). Table 2 also reports the theoretical experimental thickness (Eq. (1)) as reference value.

As expected, the 2D structural thickness yielded smaller values when compared to the cross-sectional ones although the differences are relatively small as in case of 5% w/w for Purox-S and Cellets 1000. HPMC 615 presents the lowest standard deviation (no matter the core material), meaning the highest intra-particle coating uniformity. In particular, PVA 4-98 at 1% and 5% w/w coating level presents the highest standard deviations. This insufficient intra-particle homogeneity was qualitatively confirmed looking at both the SEM cross section images in Figs. 7 and 8 and X-ray tomography 2D reconstructions in Fig. 5. HPMC 603 and PVA 4-98 give similar standard deviation. HPMC 603 and PVA 4-98 also present the largest range between max and min values of 2D cross-sectional Thickness. Additionally, no major differences were found between the mean coating thickness of coated particles at core particle (Purox-S vs. Cellets 1000) level. In fact, the coating thickness was found to be only very slightly core particle dependant. As for 2D and 3D structural thickness for 1% w/w coating level 2D cross-sectional thickness was found to overestimate the coating thickness. Beside limitations in resolutions or pixel sizes, a threshold inaccuracy for extremely thin coating shells has to be taken into account. In fact, when the coating thickness becomes smaller, the contrast between the (dark) thin coating layer and the (white) environment is also decreasing making the delineation of the coating shell more complicated and, thus, a proper threshold, not possible.

The intra-particle standard deviation for Purox-S coated particles was found to vary from low values, 0.950, in case of 9% w/w HPMC 615 to higher values, 2.32, in case of 1% w/w PVA 4-98. When Cellets 1000 are used as core material, the standard deviation is ranging from 1.017 in case of 9% w/w HPMC 615 to 2.827 in case of 1% w/w PVA 4-98.

**Table 2**
2D Cross-sectional thickness obtained by cross-sectional image analysis, the standard deviation, and values for the smallest and biggest 2D cross-sectional thickness found in the series of all 2D slices.

| Coating material | Coating level (% w/w) | Image analysis: CT analyser | | | |
|---|---|---|---|---|---|
| | | 2D Cross-sectional thickness (μm) | SD | Max (μm) | Min (μm) |
| *PUROX-S* | | | | | |
| PVA 4-98 | 1 | 2.092 | 2.320 | 3.456 | 0.000 |
| | 5 | 6.68 | 2.047 | 8.906 | 4.915 |
| | 9 | 12.563 | 1.275 | 18.873 | 11.716 |
| HPMC 603 | 1 | 2.254 | 1.958 | 3.112 | 0.000 |
| | 5 | 6.388 | 1.874 | 7.997 | 3.366 |
| | 9 | 12.37 | 1.574 | 24.378 | 10.453 |
| HPMC 615 | 1 | 2.258 | 1.669 | 3.018 | 0.000 |
| | 5 | 6.279 | 1.048 | 9.578 | 3.233 |
| | 9 | 13.093 | 0.950 | 18.785 | 11.427 |
| *CELLETS 1000* | | | | | |
| PVA 4-98 | 1 | 2.485 | 2.827 | 2.910 | 0.000 |
| | 5 | 7.874 | 2.158 | 11.546 | 4.462 |
| | 9 | 13.835 | 1.279 | 27.780 | 12.845 |
| HPMC 603 | 1 | 2.323 | 1.988 | 3.001 | 0.000 |
| | 5 | 6.821 | 1.511 | 8.012 | 2.997 |
| | 9 | 13.036 | 1.167 | 21.455 | 10.938 |
| HPMC 615 | 1 | 2.311 | 1.940 | 3.756 | 0.000 |
| | 5 | 7.312 | 1.474 | 9.410 | 4.600 |
| | 9 | 13.388 | 1.017 | 18.491 | 11.536 |

### 3.2.2. Matlab-DIPimage

As a first step the measurement error for a reference thickness of 3 pixel was calculated for all three coating thickness Matlab-DIPimage definitions, namely Surf2D and Surf3D and Avg2D. In order to evaluate the goodness of the three different definitions the measurement error for a reference thickness of 3 pixels was calculated. The results are given in Table 3 for all radii together with the standard deviation of the measurements for Surf2D and Surf3D.

Avg2D performed the worst in estimating the thickness with an overestimation of 0.6–1.01; Surf2D is better (0.7–0.84 overestimation) but still worse than Surf3D (0.08–0.11 overestimation) that has also a smaller standard deviation than Surf2D. The detailed results are: the mean average error on the thickness estimate over all tested spheres is 27%, 24% and 2.2% for Avg2D, Surf2D and Surf3D respectively. From Table 3 it is clear that the 3D method performs best and measures the average thickness correctly. The standard deviation of the measurement is a direct consequence of the realization of the sphere on a discrete grid. A possible way to improve Surf2D and Surf3D is to measure the length of the line that intersects the segmented object by a classical length estimator instead of counting the object pixels [37]. If it would be possible to measure the length not on the binarized segmented image but on the gray-value image itself a better precision could be achieved [38,39]. Unfortunately, this is not possible here as the data must be hand segmented to detect the coating properly and it touches the particle regularly. Table 4 shows the results of coating thickness determined using Avg2D, Surf2D and Surf3D definitions as described in Section 2.6.2.2. Avg2D, Surf2D and Surf3D definitions were found to overestimate the theoretical coating thickness (approximately 1.8, 1.6 and 1.3 μm respectively) for all the cases except 9% w/w coating level which is always underestimated (±9 μm vs 14–15 μm). Avg2D has been found to be 0.2–2.4 μm higher than Surf2D no matter the coating agent neither the core particle and, in the final instance, the worst one among the three definitions. Overall the standard deviation is much lower for Surf2D. No major differences could be noticed looking at the inter-particle standard deviation for different coating materials, different core particle and different coating level indicating that the coating thickness uniformity within all the particles in the analysed batches is pretty high. Nevertheless the intra-particle standard deviation of Purox-S coated particles resulted to be higher

**Table 3**
Measured thickness for a binary sphere of thickness 3 pixels with different outer radii by image analysis.

| | *Avg2D* | *Surf2D* | *Surf3D* |
|---|---|---|---|
| $r = 20$ | 3.60 | 3.70 ± 0.87 | 3.08 ± 0.37 |
| $r = 30$ | 3.77 | 3.73 ± 1.03 | 3.10 ± 0.35 |
| $r = 40$ | 3.88 | 3.75 ± 1.10 | 3.08 ± 0.37 |
| $r = 50$ | 3.96 | 3.75 ± 1.08 | 3.11 ± 0.37 |
| $r = 60$ | 4.01 | 3.84 ± 1.18 | 3.08 ± 0.36 |

**Table 4**
Coating thicknesses and the corresponding statistics obtained by Image analysis using 2D and 3D approaches.

| Coating material | Coating level (% w/w) | Image analysis: Matlab and DIPimage | | | | | | | | |
|---|---|---|---|---|---|---|---|---|---|---|
| | | Avg2D | | Surf2D | | Surf3D | | | | |
| | | Mean (μm) | STD | Mean (μm) | STD | Mean (μm) | Max (μm) | Min (μm) | STD[a] | STD [b] |
| *PUROX-S* | | | | | | | | | | |
| PVA 4-98 | 1 | 3.049 | 0.655 | 2.857 | 0.888 | 2.563 | 3.56 | 1.25 | 0.098 | 1.001 |
| | 5 | 7.646 | 0.781 | 9.045 | 0.956 | 6.873 | 6.16 | 6.14 | 0.298 | 1.336 |
| | 9 | 9.246 | 0.342 | 9.251 | 0.233 | 10.523 | 9.42 | 9 | 0.088 | 1.056 |
| HPMC 603 | 1 | 3.148 | 0.95 | 2.789 | 0.957 | 2.455 | 3.87 | 1.58 | 0.199 | 1.125 |
| | 5 | 8.574 | 1.285 | 6.111 | 0.784 | 6.569 | 8.02 | 5.7 | 0.258 | 1.182 |
| | 9 | 8.941 | 0.986 | 9.671 | 0.812 | 10.894 | 9.52 | 7.9 | 0.173 | 1.172 |
| HPMC 615 | 1 | 3.001 | 1.116 | 2.951 | 0.652 | 2.478 | 4.01 | 2.01 | 0.287 | 0.998 |
| | 5 | 5.823 | 1.323 | 7.627 | 0.638 | 6.568 | 6.76 | 5.5 | 0.138 | 0.907 |
| | 9 | 9.635 | 1.284 | 9.266 | 0.791 | 10.753 | 12 | 7.78 | 0.452 | 1.218 |
| *CELLETS 1000* | | | | | | | | | | |
| PVA 4-98 | 1 | 3.208 | 0.427 | 2.949 | 0.181 | 1.892 | 5 | 1.32 | 0.236 | 0.494 |
| | 5 | 8.347 | 1.171 | 7.157 | 0.949 | 6.413 | 6.76 | 6.16 | 0.065 | 0.718 |
| | 9 | 9.391 | 0.916 | 11.371 | 0.775 | 11.783 | 9.9 | 9.08 | 0.136 | 0.876 |
| HPMC 603 | 1 | 2.687 | 1.583 | 2.568 | 0.888 | 1.927 | 4.82 | 1.75 | 0.588 | 0.651 |
| | 5 | 8.571 | 0.937 | 8.236 | 0.76 | 6.467 | 6.94 | 6.18 | 0.118 | 0.656 |
| | 9 | 11.706 | 2.626 | 12.205 | 0.967 | 9.343 | 12.36 | 7.64 | 0.666 | 1.357 |
| HPMC 615 | 1 | 2.743 | 0.614 | 2.048 | 0.256 | 2.062 | 3.54 | 1.6 | 0.102 | 0.488 |
| | 5 | 8.368 | 0.875 | 7.951 | 0.806 | 6.719 | 8.04 | 6.16 | 0.227 | 0.776 |
| | 9 | 9.044 | 1.23 | 11.089 | 0.891 | 11. 785 | 9.52 | 6.74 | 0.328 | 0.778 |

[a] Standard deviation inter-particle.
[b] Standard deviation intra-particle.

than that from Cellets 1000 confirming the better coating quality which could be visually detected looking at the SEM and X-ray tomography images in Figs. 7, 8 and 5, respectively. Overall the coating thickness measured by using the two image analysis methods (Matlab-DIPimage vs CTAn) in both 2D and 3D are in close agreement especially with 1% and 5% w/w coating levels.

### 3.3. Structural and morphological parameters

The structure and architecture of the coating shell were also characterized by analysing the 3D reconstructed images of the coating shells. Thanks to these detailed images, the ratio between the external surface and the volume of the coating shell, $\beta$, and the surface density, $\rho$, the percent porosity, $\Phi$, the number of pores, $\Phi_{num}$, present in the coating shell, and the corresponding volume, $\Phi_{vol}$, have been calculated and reported in Table 5 for both Purox-S and Cellets 1000 coated particles. The indices are calculated for all three coating materials with respect of their coating level 1%, 5% and 9 %w/w. For percent porosity, $\Phi$, number of pores, $\Phi_{num}$ and the corresponding volume, $\Phi_{vol}$, values for single reference particle and for the whole batch are both reported for comparison.

The percent porosity, the number of pores and the corresponding volume occupied by the pores listed in Table 1 are smaller for Cellets 1000 than Purox-S. Moreover, in the Cellets 1000 case it was found that these three indices increase with increasing coating level whereas in Purox-S case an increasing in coating level is accompanied by a decrease in percent porosity, number of pores and so their occupied volume. However, in both cases HPMC 603

**Table 5**
The ratio between the external surface and the volume of the coating shell ($\beta$), the surface density ($\rho$), the percent porosity ($\Phi$), the number of pores ($\Phi_{num}$), and the corresponding volume of pores ($\Phi_{vol}$) for Purox-S and Cellets 1000 coated particles.

| Coating material | Coating level (% w/w) | $\beta$ (1/μm) | $\rho$ (1/μm) | $\Phi$ (%) | | $\Phi_{num}$ | | $\Phi_{vol}$ (μm$^3$) | |
|---|---|---|---|---|---|---|---|---|---|
| | | | | Batch | Particle | Batch | Particle | Batch | Particle |
| *PUROX-S* | | | | | | | | | |
| PVA 4-98 | 1 | 0.347 | 0.005 | 0.001 | 0.001 | 71 | 79 | 4.3E + 03 | 5.2E + 03 |
| | 5 | 1.189 | 0.004 | 0.240 | 0.241 | 17,768 | 17,798 | 2.0E + 06 | 2.0E + 06 |
| | 9 | 1.132 | 0.004 | 0.104 | 0.102 | 5822 | 6100 | 5.0E + 05 | 5.2E + 05 |
| HPMC 603 | 1 | 0.176 | 0.005 | 0.009 | 0.008 | 763 | 851 | 5.9E + 04 | 6.0E + 04 |
| | 5 | 1.210 | 0.006 | 0.111 | 0.110 | 9232 | 9497 | 8.2E + 05 | 8.4E + 05 |
| | 9 | 1.160 | 0.007 | 0.485 | 0.409 | 3405 | 4162 | 3.2E + 05 | 4.3E + 06 |
| HPMC 615 | 1 | 0.177 | 0.005 | 0.013 | 0.012 | 1093 | 1101 | 8.5E + 04 | 8.5E + 04 |
| | 5 | 2.192 | 0.006 | 0.063 | 0.069 | 5687 | 5898 | 4.4E + 05 | 5.0E + 05 |
| | 9 | 1.101 | 0.004 | 0.083 | 0.084 | 4750 | 5101 | 3.8E + 05 | 4.0E + 05 |
| *CELLETS 1000* | | | | | | | | | |
| PVA 4-98 | 1 | 0.376 | 0.0045 | 0.007 | 0.007 | 423 | 544 | 3.0E + 04 | 3.9E + 04 |
| | 5 | 0.219 | 0.0063 | 0.12 | 0.119 | 9635 | 9751 | 7.6E + 05 | 7.8E + 05 |
| | 9 | 0.126 | 0.0048 | 0.231 | 0.227 | 11,706 | 12,901 | 1.9E + 06 | 2.2E + 06 |
| HPMC 603 | 1 | 0.731 | 0.0081 | 0.0004 | 0.0009 | 14 | 21 | 2.5E + 01 | 3.1E + 01 |
| | 5 | 0.419 | 0.011 | 0.0926 | 0.091 | 5967 | 6008 | 1.7E + 04 | 1.6E + 04 |
| | 9 | 0.351 | 0.0513 | 0.816 | 0.676 | 3985 | 3293 | 6.2E + 05 | 1.8E + 05 |
| HPMC 615 | 1 | 0.925 | 0.0233 | 0.0004 | 0.001 | 12 | 28 | 8.3E + 02 | 2.5E + 02 |
| | 5 | 0.679 | 0.0442 | 0.092 | 0.076 | 5599 | 4813 | 5.6E + 05 | 4.7E + 05 |
| | 9 | 0.19 | 0.0041 | 0.106 | 0.109 | 6460 | 6859 | 5.1E + 05 | 5.4E + 05 |

seems to have the lowest values among the three coating materials. The density of the coating materials was found to be ranging between 0.0004 and 0.05 although a definitively reliable trend could be noticed.

### 3.4. Scanning electron microscope

The coated particles were also analysed using scanning electron microscope (SEM) in order to measure their coating thickness and assess the coating surface morphology and compare then such results with those obtained by using X-ray micro tomography. The thickness of the coating layer was estimated on the basis of SEM pictures by analysing at least three particles. For each particle the thickness was measured at least at five different positions. Average values are reported. The dry-basis coating fraction, the theoretical thickness [31] and the SEM-measured coating thicknesses are listed in Table 6. Fig. 7 presents scanning electron microscope cross-sections images of Purox-S coated with the three different coating agents for 1%, 5% and 9% w/w coating level. Fig. 3 gathers scanning electron microscope images of Cellets 1000 coated with the three coating agents for 1%, 5% and 9% w/w coating level. In both cases Figs. 7 and 8 per each coating agent and coating level a macro-level (200 μm), a micro-level (200 μm) and cross section are presented.

There is significant similarity between the results obtained by using SEM and those obtained by X-ray tomography for 1% and 5% coating levels. 9% coating level thicknesses measured by SEM are 5–7 μm higher instead. Compared to Matlab-DIPimage method such difference is even higher (9–10 μm approximately). The fact that only limited number of cross-sections and thus poor statistical relevance together change of coating state due to cutting and inaccuracy of hand-made measurements are likely the reason of these differences in coating thickness between SEM and X-ray micro tomography. HPMC 603 and HPMC 615 coatings show smaller standard deviations of coating thickness than PVA 4-98. Thicker coating layers were observed in proximity of "valleys" of core particle. No assumption can be made out of those pictures about the adhesion between the coating layer and the core material since the interface region was damaged during the slicing process.

The analysis of the SEM images gathered in Figs. 7 and 8 demonstrate the qualitative agreement with X-ray micro tomography of morphological parameters is in agreement qualitatively with these results. All coatings have an "orange skin" like structure. The film coating is formed by coalescence of droplets sprayed on the surface of the core particle. In some cases the droplets become dry before complete coalescence is accomplished. Moreover neither additives nor plasticisers, to help the droplets spreading, were added in the coating solutions. These lead to the formation of such bumps and craters in the coating surface. Therefore, the surfaces of the coated particles have a macroscopic and microscopic roughness. The droplet size seems to vary randomly. This could be due to variation in droplet and particle trajectory in the fluidised bed. For example, droplets will be smaller when it travels a longer distance before hitting a particle as the result of water evaporation. All process parameters were kept constant (i.e. spraying pressure, fluid bed temperature, and spraying rate) which implies that the droplet size is mainly related to the viscosity of the coating solution and the droplet trajectory and the droplet size distribution given by the spray nozzle. The surface of 1% w/w HPMC 603, HPMC 615 and PVA 4-98 coatings was less smooth and showed several irregularities both at macro-scale and micro-scale level than 5% and 9% w/w coatings. The lower uniformity and smoothness of coatings obtained from 1% w/w coatings can be explained by the relative poor amount of coating sprayed resulting in a scarce covering of the irregular shape of the Purox-S core particle. This aspect found confirmation by looking at the values of the ratio $\beta$ in Table 5. Values for 1% w/w, in fact, are always higher compared to the 5% and 9% w/w ones. Such differences are clearly visible and pronounced in case of Cellets 1000 coated particles, shown in Fig. 8 because of its spherical and regular shape.

On the other hand scanning electron microscope images of coated Cellets 1000 particles in Fig. 8 revealed better coating quality giving, in fact lower values for the ratio $\beta$ compared to those obtained for Purox-S. The coalescence of these droplets is pretty good and homogenous for all the three materials. The core particles are uniformly covered very rounded and smooth on the surface in all three cases but in some rare cases, especially for PVA 4-98 coated particles, where the droplets become dry before complete coalescence was accomplished.

In general, for both Purox-S and Cellets 1000 coated particles, the surfaces of the PVA 4-98 were rougher than the HPMC 603 and HPMC 615 coatings which were dosed at similar concentrations. All three coating materials present small cracks on their surfaces. These cracks were likely to be caused by particle–particle and particle–wall collisions during the coating process. The cracks were more evident when thicker coating layers were applied, which could be (partly) related to the residence time of the particles in the fluidised bed. The SEM images in Figs. 7 and 8 demonstrate that in the all coated particles, holes, cracks and incorporated features are present, but to a lesser extent for the Cellets 1000 coated particles when compared to the Purox-S in Fig. 7. Besides droplets there are also other structures visible on the coating surface of both Purox-S and Cellets 1000 coated particles. These structures are probably caused by the attachment of dust to the coating surface.

**Table 6**
Coating thicknesses and the corresponding standard deviations obtained by using SEM.

| Coating material | Coating level (% w/w) | Scanning electron microscope | |
|---|---|---|---|
| | | Mean[a] (μm) | STD |
| *PUROX-S* | | | |
| PVA 4-98 | 1 | 1.4 | 2.1 |
| | 5 | 7 | 2.5 |
| | 9 | 20.2 | 2.9 |
| HPMC 603 | 1 | 2 | 2 |
| | 5 | 8.5 | 1.9 |
| | 9 | 20.5 | 3 |
| HPMC 615 | 1 | 2.1 | 1.8 |
| | 5 | 8.8 | 2.8 |
| | 9 | 21 | 2.5 |
| *CELLETS 1000* | | | |
| PVA 4-98 | 1 | 1.5 | 1.5 |
| | 5 | 7.1 | 1.6 |
| | 9 | 19.9 | 1.9 |
| HPMC 603 | 1 | 1.6 | 1.7 |
| | 5 | 6.9 | 1.7 |
| | 9 | 20.8 | 2.1 |
| HPMC 615 | 1 | 1.6 | 1.8 |
| | 5 | 8.3 | 2.2 |
| | 9 | 20.9 | 1.9 |

[a] Ref. [40].

## 4. Discussion

The values of the coating thickness obtained by X-ray micro tomography has a much higher statistical reliability compared to SEM, being measured over the all perimeter, per each of the 575–600 2D reconstructed images. Moreover the 2D reconstructed images in Fig. 5 and the 3D reconstructed images in Fig. 6 gives a much better overview of the real status of the adhesion between core particle and coating layer. Detachments of the coating layer from the core particle visible in Figs. 7 and 8 could be easily due

to the cutting of the section and thus be an artificial feature. This problem is definitely not an issue for X-ray micro tomography leading to more precise and reliable information.

The SEM images show that HPMC 603, HPMC 615 and PVA 4-98 have got similar internal structure although could not quantify porosity, density or the ratio surface/volume. SEM was, thus, able to give qualitative information about the structure of coating shells, although destructively. Moreover in order to get sufficient information for statistical analysis, the scanning process would have to be repeated many times using different samples, since multiple slicing of the same sample would be extremely difficult in this case due to the delicate nature of the coating shell, especially in 1% w/w coating level cases. For X-ray micro tomography, instead, in a given single scan, the ratio of the height of the sample to the resolution of the scan represents the total number of 2D horizontal images that can be reconstructed, without any physical slicing required. In this case, the scan generated a total of 575/600 2D horizontal images. The reconstructed images, thus obtained, were used to render the real 3D model of the samples, as already shown in Fig. 4. The 3D model can then be sliced at any level, in any direction in order to view the inner structure of the material. Such a feature makes X-ray micro tomography ideally suited for the non-invasive imaging of such samples, especially those with a delicate structure such as fragile coated particles and, thus, gives it a leading edge over other techniques such as SEM. Moreover, the border between coating layer and core particle is very clear and an idea about the density-structure of the sample can be derived based on the intensity of the gray values. On the other hand 2 μm resolution makes the detection and calculation of few microns coating thickness not really reliable and accurate.

Overall the combination of SEM and micro-CT can offer important information concerning the structure and morphology of the coating layer, the localization of the pores and the calculation of coating thickness. While micro-CT can monitor very well changes in 3D, the SEM will give detailed 2D information. As matter of fact, both techniques are complementary and using them both provides important extra information. As result of rapid technology improvements, the resolution of X-ray micro tomography will be enhanced up to nano-scale by the development of nano-CT making 2D and 3D analysis even more detailed.

In comparison with the conventional SEM micrograph (Figs. 3 and 4) the digital slices obtained by X-ray micro tomography (Figs. 7 and 8) offer higher contrast as well as much more detailed structural information.

However regarding 1% w/w coated Purox-S and 1% w/w coated Cellets 1000 the resolution of the X-ray micro tomography is not high enough to have a statistical reliability and to distinguish the coating layer in the same detail as SEM (Figs. 5, 7 and 8). On the other hand, the images derived from the X-ray micro tomography indicate a global overview of the sample in 3D with the distribution of the coating agent onto the core particle and in particular at the interface.

## 5. Conclusions

This work reviews X-ray micro tomography as a powerful non-destructive technique for the micro structural characterization of coated particles and to reveal details and characteristics of the coating shell. X-ray micro tomography gives the possibility to examine the internal structure in both 2D and 3D. 3D analysis, in particular, represents a step further considering the classical visualization techniques. X-ray micro tomography was shown to be an excellent tool to visualize and unambiguously identify and quantify eventual cracks, damages inside or on the surface of the particles and to calculate parameters such as surface density, porosity and coating thickness. This is hardly possible by other methods. The amount and the quality of the information obtained (several particles in one test), the details level, the possibility to look at the structures internally, the relatively easy implementation were found to be the strengths of the technique. Moreover, the high reproducibility, the 3D visualization and the fact that any fluorescent agent has to be used make this technique preferable when compared to other techniques. On the other hand its high costs, the limits in resolution (which depends on the X-ray equipment used though) and not applicability for rapid in-process or at-line monitoring makes this technique not suitable for daily quality control. Additionally the ability to obtain sharp, well resolved and good contrast images depends on the difference in density and atomic number of the objects in exam which sometimes can be low and, thus, lead to poor-quality images.

Both the structural characteristics (the ratio solid surface-volume ($\beta$), the surface density ($\rho$), the number of pores ($\Phi_{num}$) in the coating shell, the corresponding volume ($\Phi_{vol}$), occupied and the percentage porosity ($\Phi$) and the coating thickness (CT Analyser and Matlab-DIPimage) of the coated particles were determined at different levels of detail using 2D and 3D approaches in the analysis. By analysing the data (both mean values and standard deviations), X-ray micro tomography was demonstrated to be a reliable tool to control the final quality of the products, to continue improvement of the coating process, to gain knowledge about the evolution of coating film-forming, and even to qualitatively predict final performances and variations in release rate due to geometrical variations in the particles.

## References

[1] M. Andersson, M. Josefson, F.W. Langkilde, K.G. Wahlund, Monitoring of a film coating process for tablets using near infrared reflectance spectroscopy, J. Pharm. Biomed. 20 (1999) 27–37.
[2] M. Andersson, B. Holmquist, J. Lindquist, O. Nilsson, K.G. Wahlund, Analysis of film coating thickness and surface area of pharmaceutical pellets using fluorescence microscopy and image analysis, J. Pharm. Biomed. 22 (2000) 325–339.
[3] K. Nienaltowska, G. Perfetti, G. Meesters, F. Ronsse, J.G. Pieters, K. Dewettinck, F. Depypere, Attrition strength of water-soluble cellulose derivatives coatings, Powder Technol. 198 (2010) 298–309.
[4] L. Felton, J.W. McGinity, Adhesion of polymeric films to pharmaceutical solids, Eur. J. Pharm. Biopharm. 47 (1999) 3–14.
[5] S. Missaghi, R. Fassihi, A novel approach in the assessment of polymeric film formation and film adhesion on different pharmaceutical solid substrates, AAPS PharmSciTech. 5 (2004). article 29.
[6] B.R. Mathews, J.R. Nixon, Surface characteristics of gelatin microcapsules by scanning electron microscopy, J. Pharm. Pharmacol. 26 (1974) 383–384.
[7] M. Kalab, Practical aspects of electron-microscopy in dairy research, Food Struct. 12 (1993) 95–114.
[8] M. Kalab, P. Allan-Wojtas, S.S. Miller, Microscopy and other imaging techniques in food structure analysis, Trends Food Sci. Technol. 6 (1995) 177–186.
[9] W. Plugge, C. Van Der Vlies, The use of near infrared spectroscopy in the quality control laboratory of the pharmaceutical industry, J. Pharm. Biomed. Anal. 10 (1992) 797–803.
[10] B.F. MacDonald, K.A. Prebble, Some applications of near-infrared reflectance analysis in the pharmaceutical industry, J. Pharm. Biomed. Anal. 11 (1993) 1077–1085.
[11] J.D. Kirsch, J.K. Drennen, Determination of film-coated tablet parameters by near-infrared spectroscopy, J. Pharm. Biomed. Anal. 13 (1995) 1273–1281.
[12] A.M. Healy, O.I. Corrigan, J.E.M. Allan, The effect of dissolution on the surface texture of model solid-dosage forms as assessed by noncontact laser profilometry, Pharm. Technol. Eur. 9 (1995) 14–22.
[13] Y. Mouget, P. Gosselin, M. Tourigny, S. Bechard, Three-dimensional analyses of tablet content and film coating uniformity by laser-induced breakdown spectroscopy (LIBS), Am. Lab. 2 (2003) 20–22.
[14] E. Fekete, B. Pukánszky, A. Tóth, I. Bertóti, Surface modification and characterization of particulate mineral fillers, J. Colloid Interf. Sci. 135 (1990) 200–208.
[15] J.C.G. Blonk, H. Van Aalst, Confocal scanning light microscopy in food research, Food. Res. Inst. 26 (1993) 297–311.
[16] A. Boyde, Bibliography on confocal microscopy and its applications, Scanning 16 (1994) 33–56.

[17] J.C.G. Blonk, J. Van Eendenburg, M.M.G. Koning, P.C.M. Weisenborn, C. Winkel, A new CSLM-based method for determination of the phase behaviour of aqueous mixtures of biopolymers, Carbohydr. Polym. 28 (1995) 287–295.
[18] Y. Vodovotz, E. Vittandini, J. Coupland, D.J. Mcclements, P. Chinachoti, Bridging the gap: use of confocal microscopy in food research, Food Technol. 50 (1996) 76–82.
[19] M. Ferrando, W.E.L. Spiess, Review: confocal scanning laser microscopy. A powerful tool in food science, Food Sci. Technol. Int. 6 (2000) 267–284.
[20] M.B. Dürrenberger, S. Handschin, B. Conde-Petit, F. Escher, Visualization of food structure by confocal laser scanning mcroscopy (CLSM), Lebensm.-Wiss. u.-Technol. 34 (2001) 11–17.
[21] F. Depypere, P. Van Oostveldt, J.G. Pieters, K. Dewettinck, Quantification of microparticle coating quality by confocal laser scanning microscopy (CLSM), Eur. J. Pharm. Biopharm. 73 (2009) 179–186.
[22] A. Lamprecht, U.F. Schafer, C.M. Lehr, Visualization and quantification of polymer distribution in microcapsules by confocal laser scanning microscopy (CLSM), Int. J. Pharm. 196 (2000) 223–226.
[23] A. Lamprecht, U.F. Schafer, C.M. Lehr, Structural analysis of microparticles by confocal laser scanning microscopy, AAPS PharmSciTech 1 (2000). article 17.
[24] A. Sasov, Microtomography, J. Microsc. 147 (1987) 169–192.
[25] A. Sasov, D. Van Dyck, Desktop X-ray microscopy and microtomography, J. Microsc. 191 (1998) 151–158.
[26] G. Perfetti, K.M.B. Jansen, W.J. Wildeboer, P. van Hee, G.M.H. Meesters, Characterization of physical and viscoelastic properties of polymer films for coating applications under different temperature of drying and storage, Int. J. Pharm. 384 (2010) 109–119.
[27] G. Perfetti, J. Arfsten, A. Kwade, W.J. Wildeboer, G.M.H. Meesters, Repeated impacts tests and nanoindentation as complementary tools for mechanical characterization of polymer-coated particles, J. Appl. Polym. Sci. 118 (2010) 790–804.
[28] L.A. Feldkamp, L.C. Davis, J.W. Kress, Practical cone beam algorithm, J. Microsc. 185 (1997) 67–75.
[29] Skyscan, Structural parameters measured by Skyscan™ CT-analyser software, 2008.
[30] W.E. Lorensen, H.E. Cline, Marching cubes: a high resolution 3D surface construction algorithm, Comput. Graphics 21 (1987) 163–169.
[31] K. Dewettinck, L. Deroo, W. Messens, A. Huyghebaert, Agglomeration tendency during top-spray fluidized bed coating with gums, Lebensm.-Wiss. u.-Technol. 31 (1998) 576–584.
[32] A. M Parfitt, M.K. Drezner, F.H. Glorieux, J.A. Kanis, H. Malluche, P.J. Meunier, S.M. Ott, R.R. Recker, Bone histomorphometry: standardization of nomenclature symbols and units, J. Bone Miner. Res. 2 (1987) 595–610.
[33] W.K. Pratt, Digital Image Processing, second ed., Wiley, New York, 1991.
[34] T. Hildebrand, P. Ruegsegger, A new method for the model independent assessment of thickness in three dimensional images, J. Microsc. 185 (1997) 67–75.
[35] E. Remy, E. Thiel, Medial axis for chamfer distances: computing look – up tables and neighbourhoods in 2D or 3D, Pattern Recognit. Lett. 23 (2002) 649–661.
[36] J.P. Serra, Image Analysis and Mathematical Morphology, vol. 1, Academic Press, London, 1984.
[37] A.M. Vossepoel, A.W.M. Smeulders, Computer graphics and image processing 20 (1982) 347–364.
[38] P.W. Verbeek, L.J. van Vliet, An estimator of edge length and surface area in digitized 2D and 3D images, Proc. 11th IAPR Int. Conf. on Pattern Recognition 3 (1992) 1–5.
[39] B. Rieger, F.J. Timmermans, L.J. van Vliet, P.W. Verbeek, On curvature estimation of iso-surfaces in 3D gray-value images and the computation of shape descriptors, IEEE Trans. Pattern Anal. Mach. Intell. 26 (2004) 1088–1094.
[40] G. Perfetti, T. Aubert, W.J. Wildeboer, G.M.H. Meesters, Influence of handling and storage conditions on morphological and mechanical properties of polymer-coated particles: characterization and modelling, Powder Technol. (2010), doi:10.1016/j.powtec.2010.03.040.